PROCEEDINGS of the
24th International Congress on Acoustics

October 24 to 28, 2022 in Gyeongju, Korea

ABS-0158

Experimental and Numerical Advances in Underwater Radiated Noise Prediction of Cavitating Propeller-Hull Combinations

Julian KIMMERL[1]; Paul MERTES[2]; Vladimir KRASILNIKOV[3]; Kourosh KOUSHAN[3]; Luca SAVIO[3]; Mario FELLI[4]; Moustafa ABDEL-MAKSOUD[5]; Nils REICHSTEIN[6]

[1] Hydrodynamics & Propeller Design, SCHOTTEL GmbH, Germany

[2] Technical Support Navy & Governmental, SCHOTTEL GmbH, Germany

[3] Dept. of Ships and Ocean Structures, SINTEF Ocean, Norway

[4] Hydrodynamics and Hydroacoustics Dept., Institute of Marine Engineering (INM) – National Research Council (CNR), Italy

[5] Institute for Fluid Dynamics and Ship Theory, Hamburg University of Technology (TUHH), Germany

[6] Strength, Vibration, Acoustics and Shock, Fr. Lürssen Werft GmbH & Co. KG, Germany

ABSTRACT

Propeller induced cavitation is the primary underwater radiated noise source of motorized shipping activities, which coincides with acoustic frequencies utilized by marine life and may therefore have negative impacts on the ecosystem. This paper is the conclusion of the research project ProNoVi introduced at ICA2019 and presents the final results of both experimental and numerical campaigns on a high-level for all participants. While propulsion related phenomena are analyzed based on evaluation of high-speed recordings, the focus lies on model and full scale comparisons of acoustic measurements with pressure pick-ups and hydrophones in the far-field. Accompanying simulations with active phase transition are undertaken, by employing high fidelity CFD methods with RANS and scale resolved DES or LES turbulence modelling. For different methods and setups, the emitted noise from the propeller and its slipstream, where induced vorticity and cavitation-dynamics play an important role, are compared for an openwater propeller case and several propeller-hull combinations. The analysis of these workflows on real propeller-ship combinations reveal adequate results, regarding comparability and reproducibility between different experimental and numerical setups and point to future opportunities for the improvement of accurate underwater noise predictions while saving numerical and experimental resources.

Keywords: Underwater radiated noise, Marine propeller, Cavitation, CFD, Experiment

1. INTRODUCTION

1.1 URN as Environmental Issue

The spectral background underwater noise characteristics in the earth's oceans are primarily affected by anthropogenic noise due to shipping activities in the medium frequency ranges. Oceanic shipping increases the amplitudes of the medium frequency bands between 10Hz and 1000Hz up to 30dB (1). In general, commercial shipping is, depending on regional circumstances, the dominating part of the underwater overall noise levels, although it has to be considered that acoustic sensitivity of distinct species may depend on season and frequency range. An overlap between typical shipping noise and frequencies required for communication, as well as effective predator-prey interaction, is verified, e.g. for the species Catacea (2), Testudines (3) and Elasmobranchii (4). Due to the long life-span of some of the affected species, the changes in the background noise level occurred in an evolutionary neglectable timeframe, which may lead to adverse effects on their natural behavior. This could lead to significant detriments on their life strategies, possibly leading to extinction of species,

[1] jkimmerl@schottel.de

which is cause for the inclusion in some regulatory bodies' rules and guidelines, such as the EU commission and the IMO (5). In some cases, these are translated to a local level by regional regulations with operational implications for the industry, e.g. as implemented by the Port of Vancouver (6).

To attack the problem effectively, shipping noises require to be differentiated between its sources and their corresponding frequency ranges, with multiple acoustic emitters on vessels such as propulsion, engines, gear boxes, pumps and hydraulic aggregates. The most important noise source over a wide frequency range is the propulsion, once the vessel speed for onset of cavitation is exceeded or when operated in off-design conditions, as the imploding large sheet and vortex cavity regions and the separating single bubbles are the main contributors to broadband noise. Propulsion devices may be studied individually, however, in reality they are part of a complex system consisting of the ship's hull, which affects the inflow and generally the turbulent flow field in which the propulsor is operating, and some form of rudder instrumentation, which typically operates behind the propulsor, due to increased steering forces for this position and is affected by the highly turbulent propeller slipstream. For a recent overview of the state of the art see Kimmerl or Krasilnikov (7,8).

1.2 ProNoVi Project

The project ProNoVi - "Analysis Methods and Design Measures for the Reduction of Noise and Vibration Induced by Marine Propellers", as part of the EU-commissions MarTERA ERA-NET cofund, investigates the effects of the aforementioned interactions occurring for a propeller operating in behind ship condition on the acoustic emissions and aims to develop experimental and numerical methods and standards for practical application in an industry environment. For this purpose the target cases shown in Figure 1, a $L_s = 130m$ twin-screw mega yacht with fixed pitch propellers, a $L_s = 145m$ single-screw container ship with controllable pitch propellers and a $L_s = 24m$ fast twin-screw catamaran for servicing wind farms, are investigated. The consortium consisting of the research partners SINTEF-Ocean and CNR-INM, the academic partner Technical University Hamburg and three industry partners Lürssen, Schottel and Helseth with their respective target cases. The first vessel (a) is invoked as a reference target case and thus studied in experimental measurements in full scale and two different model scale configurations, with a half-model considering the ships centerline symmetry plane and a full-model with two propellers respectively. Numerically two contrary approaches for evaluating the flow field are followed, with finite volume methods, both Reynolds averaged (RANS) and high-fidelity turbulence resolving (DES, LES) are utilized, and a boundary element method, specifically a panel method. This allows for both highly iterative propeller design tasks requiring fast calculations and detailed investigations of noise generation mechanisms with higher numerical resource requirements. The multitude of investigations yield the possibility to ascertain testing facility influence, repeatability of experimental and numerical investigation with different arrangements, practical applicability of scaling methods, and accuracy of numerical methods for different geometrical scales and turbulence modelling approaches. Several operation conditions are analyzed for openwater, with straight and oblique inflow, and behind hull configuration, in wetted and cavitating conditions.

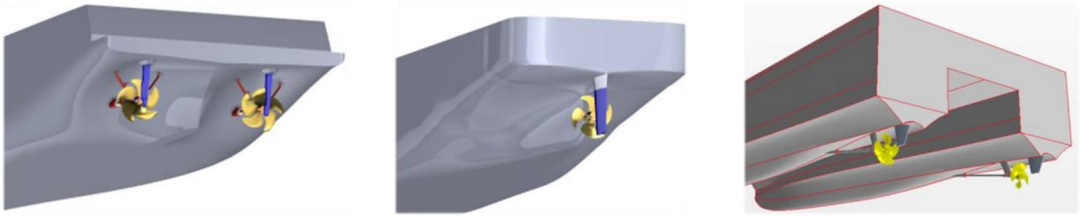

(a) Mega yacht Lürssen | (b) Container ship Schottel | (c) Wind farm service catamaran Helseth

Figure 1 – ProNoVi Target Cases

2. METHODS

2.1 Experimental

Three different experimental configurations are considered, where the main difficulties lie in the inherent dependence of underwater noise on geometrical characteristics of each. As a result, it is

common practice to apply a number of corrections to any noise measurements.

2.1.1 Model Scale

The measurements at SINTEF Ocean with a port side half hull model are performed in the Large Cavitation Tunnel featuring a test section size of $6.0m \cdot 1.3m \cdot 1.2m$ described by a model center plane and a wooden top plate near the waterline. LDV equipment is mounted on the side window at the propeller plane, the pressure pick-ups have a sampling frequency of 9.6kHz with a filter cut-off frequency of $2.0kHz$. A Broeel & Kjaer model 8103 hydrophone is located inside a hydrofoil in the test section and records with $96.0Hz$. There are three cameras (black) and two high speed cameras (green), with a sampling rate of 2kHz to allow for 6° interval resolution, located with a clear view of the propeller as shown in Figure 2. A transfer function is obtained by measuring background noise and gross noise in order to obtain the propeller net acoustic emissions.

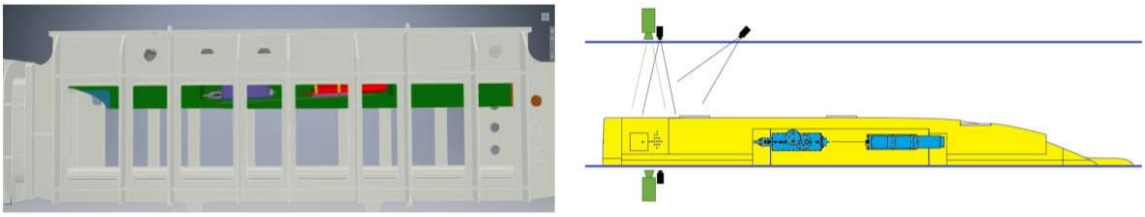

Figure 2 – SINTEF test section and experimental setup

CNR-INM measurements are conducted on a full hull model in the Large Cavitation Channel of CNR-INM[2] with dimensions of $10m \cdot 3.6m \cdot 2.25m$ at the test section as shown in Figure 3 with a free water surface. The set up consists of two hydrophones positioned in correspondence of the propeller plane with H1 located $112cm$ beside the propeller axis on the starboard side and H2 located $140cm$ below the propeller axis in correspondence of the facility midplane. Additionally, nine pressure gauges are located on the hull as indicated in Figure 4. The hydrophones are miniature, high-sensitivity transducers by Brüel & Kjær of the model B&K 8103 with a frequency range of $0.1Hz - 180kHz$ and a sensitivity of $-211dB\ re\ 1V/\mu Pa$. Hydrophone signals are conditioned by a Brüel & Kjær "NEXUS" charge amplifier and then acquired by a 20 channel-24 bit DAW PROSIG P8200. The pressure gauges are dynamic pressure transducers by PCB, i.e. PCB 106B with a frequency range of $0.5Hz - 60kHz$ and a sensitivity of $43.5mV/kPa$, flush mounted to the hull vault through dedicated metallic inserts. Pressure signals are recorded for a time window of $\Delta T = 90s$ at the sampling frequency of $f_s = 100kHz$. Cavitation observations are performed through a high-speed camera by Photron (Photron SAx1 model), rotated by 45° along the vertical axis directed at the starboard propeller from one side through a 45° inclined water prism attached to the facility window. The illumination is provided by a $1800W$ high-intensity HMI lamp by ARRI and a $1000W$ halogen lamp by DEDOLIGHT. For the experimental results, transfer functions are calculated with background noise measurements, which are applied to the propeller measurements, in order to obtain propeller net noise.

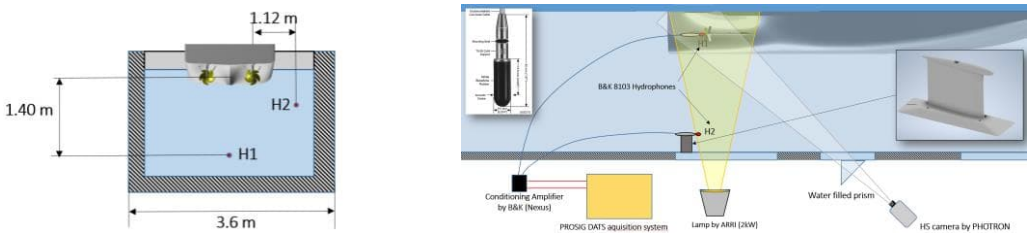

Figure 3 – CNR-INM test section and experimental setup

2.1.2 Full Scale

Full scale measurements of the reference target case mega yacht are done from a work boat, which is free floating with all engines stopped and power supply from batteries only. The distance to the track of the yacht passing by is $113m$ in the first passage and $270m$ in the second passage. Noise measurements are conducted with a freely suspended hydrophone. The calibration of the measurement chain is conducted on scene by a pistonphone with a frequency of $250Hz$. The depth of the hydrophone is determined by measurements of the static pressure at the hydrophone and is calculated

[2] www.inm.cnr.it/labs/circulating-water-channel/

from the cable angle at water surface, cable geometry, ballast and cable length, leading to a corrected distance between noise source and observer. Data acquisition is done with a National Instruments suite, the signal analysis done in Matlab. A pressure sensor type Cera Diver from Van Essen Instruments is used. GPS position of the hydrophone is recorded with a Garmin GPS and ship position is tracked from the AIS signal. A Leica range master is used for additional optical control of the distance from the yacht at closest point of approach.

The measured received levels of underwater radiated noise are converted to monopole source levels accounting for the Lloyd's Mirror effect using the following information:

- Water depth from echo sounder of the yacht
- Source depth from technical data of the propeller and ship general arrangement
- Hydrophone depth calculated from submerged cable length and cable angle at the water surface
- Distance ship-hydrophone calculated from GPS-data of the target ship and from mobile GPS receiver at the hydrophone cable attachment point
- Nature of the soil from a geological map

2.2 Numerical

The general challenges associated with the numerical investigations are: the resolution of the propeller cavitation in particular for the trailing vortices, oblique and thus temporally and spatially unsteady inflow, and respecting the vessel wakefield as well as the rudder. While finite volume methods aspire to resolve turbulence and trailing vortices in exchange for larger numerical resources, the boundary element method is required as a feasible way for implementation into recurring industry workflows.

2.2.1 Finite Volume Method

In ProNoVi, two software solutions for the finite volume methods are used, HELYX-core, an OpenFOAM distribution, with the solver interPhaseChangeDyMFoam and StarCCM+. As a propeller rotating with respect to a fixed ship hull is an intrinsically transient phenomenon, a full propeller model and an unsteady PIMPLE simulation scheme is utilized for the finite volume approaches, in both openwater and behind hull conditions. The propeller rotation is realized with a sliding mesh interface in the form of a cylinder with its rotational axis along the propeller shaftline with one base located upstream between propeller and shaft brackets and the other downstream between the propeller hub cap and the rudder location.

Turbulence modelling is differentiated between isotropic RANS modelling, which employs two equation models with either a fully turbulent k-ω-SST or a $\gamma - Re_\theta$ transition approach. For the high-fidelity simulations, the turbulence is resolved with LES, either implicit or with Smagorinsky subgridscale modelling for OpenFOAM. As a hybrid approach the improved delayed DES is applied with a delay factor for enhancing the differentiation between RANS and LES on highly refined meshes and based on an improved formulation with subgrid length scales depending on wall distance, which is applied for the StarCCM+ approach.

Regarding the physical transport properties an incompressible, isothermal two-phase homogeneous Eulerian mixture model for water and vapor with volume of fluid phase-fraction capturing is utilized as a volume-of-fluid method (VOF), where the mass and momentum transport equations of the fluid mixture are solved. One additional scalar transport equation for the water volume phase fraction α to scale the physical properties is required with a source term for cavitation on the right-hand side

$$\frac{\partial \alpha}{\partial t} + \nabla \cdot (\alpha \vec{u}) + \nabla \cdot [\alpha(1-\alpha)u_c\,] = \frac{\dot{m}}{\rho_l}, \tag{1}$$

where u_c is an artificial velocity field to compress the interface. Phase transition is modelled with the Schnerr-Sauer cavitation model (9), based on a simplified Rayleigh-Plesset equation

$$R\frac{d^2R}{dt^2} + \frac{3}{2}\left(\frac{dR}{dt}\right)^2 = \frac{p(R)-p_\infty}{\rho_l} - \frac{2\sigma}{\rho_l R} - \frac{\frac{4\mu}{\rho_l R}dR}{dt}. \tag{2}$$

In the respective implementations, the vaporization and condensation coefficients C_v and C_c are set to unity, the bubble radius is R, the nucleation volume fraction α_{Nuc}, and the nuclei density $n_0 = 1 \cdot 10^{12} m^{-3}$ and initial nuclei diameter $d_{Nuc} = 1 \cdot 10^{-4}$ (OpenFOAM) and $d_{Nuc} = 1 \cdot 10^{-6}$ (StarCCM+) respectively. Both OpenFOAM and StarCCM+ with their implicit LES and IDDES are proven to be able to resolve trailing vortices with sufficient mesh refinement in regions of high

vorticity. (7,8)

2.2.2 Panel Method

The panel method *pan*MARE is a boundary element spatial discretization for potential flow based on the work published by Katz and Plotkin (10). It is based on the conservation equation of two potentials in the fluid volume. After some transformations, a Neumann form of the equation is reached containing the inflow velocities $\vec{v}_M$ and external potentials due to waves etc. The function Φ_{ext} as well as the surface properties called doublet strength μ and source strength σ, which are used to substitute the potential on the surface and its derivative in normal direction respectively

$$0 = \underbrace{\frac{1}{4\pi}\int_{S_B}\left[\nabla\mu\frac{\partial}{\partial n}\frac{1}{r}\cdot\vec{n} - \nabla\sigma\frac{1}{r}\cdot\vec{n}\right]dS}_{\nabla\Phi_{ind}} - \underbrace{\nabla\Phi_M}_{=\vec{v}_M}\cdot\vec{n} + \nabla\Phi_{ext}\cdot\vec{n}. \tag{3}$$

After solving the resulting equation system, the total velocity $\vec{v}^*$ at every location in the simulation domain can be determined

$$\vec{v}^* = \nabla(\Phi_{ind} + \Phi_{ext} + \Phi_M), \tag{4}$$

as well as the corresponding pressure

$$p = \rho\left[\vec{g}\cdot(\vec{P}_\infty - \vec{P}) - \underbrace{\frac{1}{2}(\nabla\Phi_{ind} - \nabla\Phi_M + \nabla\Phi_{ext})^2}_{=\frac{1}{2}\vec{v}_{local}^2} - \frac{\partial(\Phi_{ind}+\Phi_{ext})}{\partial t} + \underbrace{\frac{1}{2}(\nabla\Phi_M)^2}_{=\frac{1}{2}\vec{v}_M^2}\right] + p_\infty, \tag{5}$$

at its location $\vec{P}$. The partially nonlinear model implemented in *pan*MARE for sheet cavitation is based on Fine (11). On panels identified as cavitating, the doublet strengths are determined by rearranging the Bernoulli equation and integrating the main velocity component to fulfil the dynamic boundary condition. This is done in a predictor-corrector approach multiple times in one time step. The cavity thickness is calculated by solving an explicit equation system implementing the kinematic boundary condition, which requires the cavity surface to be a material surface in the flow.

2.2.3 Acoustic Analogy

To consider acoustic effects the integral permeable surface Ffowcs Williams-Hawkings method (12) in the Farassat 1A formulation, based on a generalized Lighthill acoustic analogy, which respects solid boundary and uniform convection effects, is applied to the flow simulation results for the far-field observer. This method is derived from the compressible Navier-Stokes equations under assumption of a non-viscous medium and reduces the acoustic pressure sources to a non-deformable control surface around the relevant flow structures

$$p'(\vec{x},t^*) = p'_T(\vec{x},t^*) + p'_L(\vec{x},t^*) + p'_Q(\vec{x},t^*), \tag{6}$$

which are distinguished by type as pseudo-thickness p'_T

$$p'_T(\vec{x},t^*) = \frac{1}{4\pi}\frac{\partial}{\partial t}\int_S\left[\frac{\rho_0 u_n + (\rho-\rho_0)(u_n-v_n)}{r|1-M_r|}\right]_{ret}dS, \tag{7}$$

and -loading p'_L

$$p'_L(\vec{x},t^*) = \frac{1}{4\pi}\frac{1}{c}\frac{\partial}{\partial t}\int_S\left[\frac{P'_{nr}+\rho u_r(u_n-v_n)}{r|1-M_r|}\right]_{ret}dS + \frac{1}{4\pi}\int_S\left[\frac{P'_{nr}+\rho u_r(u_n-v_n)}{r^2|1-M_r|}\right]_{ret}dS, \tag{8}$$

whose terminology is originating in rotational noise, as well as quadrupole sources p'_Q

$$p'_Q(\vec{x},t^*) = \frac{1}{4\pi}\frac{1}{c^2}\frac{\partial^2}{\partial t^2}\int_V\left[\frac{T_{rr}}{r|1-M_r|}\right]_{ret}dV + \frac{1}{4\pi}\frac{1}{c}\frac{\partial}{\partial t}\int_V\left[\frac{3T_{rr}-T_{ii}}{r^2|1-M_r|}\right]_{ret}dV + \int_V\left[\frac{3T_{rr}-T_{ii}}{r^3|1-M_r|}\right]_{ret}dV, \tag{9}$$

with the Lighthill stress tensor T. For the reconstruction of the acoustic signal, the individual contributions are evaluated at the retarded time $t^* = t - r/c$, which is the reason that predetermined observers are selected for the evaluation step. The various approaches in this investigation apply different simplifications, such as respecting a stationary control surface or neglecting the quadrupole contributions of Eq. (9). While in HELYX and *pan*MARE, the evaluation is executed at runtime and only observer signals are reported, the complete control surface is stored for all timesteps in the StarCCM+ implementation so the acoustic observers may be selected as part of the post-processing.

For the analysis, the control surface is cylindrical around the propeller with the main axis colinear to the rotation axis or a rectangular box around the propeller and rudder. In the finite volume methods, an additional difficulty is presented in the restrictions by the sliding mesh interface, as the control surface requires a stationary underlying mesh and thus is located between the sliding interface and the

surrounding appendages. While the quadrupole sources outside the control surface are neglected for all approaches, StarCCM+ also calculates the quadrupole sources inside the control volume defined by the surface.

2.3 Acoustic Post-Processing and Comparison

A standard FFT algorithm is applied to the time series data, followed by a conversion to a single sided spectrum and respective correction factors for energy preservation and windowing. Model scale pressure signals are scaled to full scale for improved comparability with

$$P_s = P_m \left[\left(\frac{n_s D_s}{n_m D_m} \right)^2 \frac{\rho_s r_m D_s}{\rho_m r_s D_m} \right], \tag{10}$$

where the subscript s indicates full scale and m model scale values. Similarly, frequencies are scaled with $F_s = F_m n_S / n_m$. For the 1/3 octave band representations a domain band pass filter is applied on the experimental results, while the data obtained from numerical results is synthesized from discrete narrowband data in frequency domain.

The comparison of hull pressure pulses at propeller blade harmonics evaluates the closest distance discrete frequency point in the set. For spectral far-field comparison the observer signals in $dB\,re\,1 \cdot 10^{-6} Pa$ are converted to normalized source level signals with

$$RNL = SPL + 20 \log_{10}(r_m / r_s) \tag{11}$$

at $r_s = 1m$.

3. TEST CASE

Two main operation points for the comparison of the different methods are selected. Coordinate systems are cartesian with their origin at the intersection of the propeller plane and the rotational axis, with the positive x-axis directed upstream and the positive z-axis against the gravitation force.

3.1 Propellers and operation points

Two different test cases are considered in Table 2, with one being the public domain propeller P1595 for the openwater test and the second the confidential P3193 propeller geometry in behind hull condition with a scaling factor of $\lambda = 21.078$. The coordinate origin for each is at the intersection of the propeller shaft axis and the propeller plane, which is the center of the cavitation tunnel and the numerical domains for the openwater cases. In both cases the inflow speed and thus the advance ratio J are not measured and the propeller thrust is the defining setting parameter.

To evaluate the consistency of the used methods, first the P1595 propeller geometry in model scale with a shaft angle of $\varphi = 0°$ is compared in open water condition. The location of the hydrophone $\vec{x} = (0.035,\ 0.4, 0.128)$ in the experimental investigations, is considered far-field, for a wavelength of $3\lambda_f$, leading to a frequency above $f > 7.1Hz$. The operation point is at $k_T = 0.302$ with $J = 0.60$ for a rotation rate of $n = 30Hz$ and a cavitation number of $\sigma_n = 2.00$, which features a well-developed cavitating tip and hub vortex, as well as significant amount of sheet cavitation on the suction side starting at the leading edge. While the experiments each have different cavitation tunnel geometries, the OpenFOAM setup considers the SINTEF cavitation tunnel walls, and StarCCM+ and panMARE employ a quasi-infinite domain without walls.

To ensure comparability to the full scale measurements, the second comparison focuses on the P3193 propeller geometry given in Table 2 in combination with the reference target case hull with a shaft inclination of 2.75°. For the full scale measurement and the respective numerical comparisons, the operation point is $J \approx 0.82$ and $\sigma_n = 1.38$, designated C1 with the hydrophone position at $\vec{x} = (0,\ 150, 0)$ given by the full scale experimental setup. The considered model scale operation point C2 is $k_T = 0.267$ and $\sigma_n = 1.2$, leading to an inflow speed corresponding to around $J = 0.6 - 0.7$. The hydrophone location in the model experiments is $\vec{x} = (0.095,\ 0.037, -0.36)$, which can be considered far-field for frequencies $f > 8Hz$.

Table 2 – Propeller main parameters

Parameter	Unit	P1595	P3193
Diameter	$[m]$	0.204	0.204
Pitch ratio	$[-]$	1.188	1.061
Area ratio	$[-]$	0.626	0.849

Table 3 – Setups with hull

Type	Boundary Conditions	Mesh
FVM	Velocity inlet / pressure outlet / walls	$\sim 25 \cdot 10^6$ cells $\sim 1.2 \cdot 10^6$ faces propeller

Skew	[°]	42	42
Number of	[−]	4	5

Panel method	Axial projection vessel wakefield / constant dipole and source strength	4200 panels propeller 19200 panels propeller wake
	Experiment operation	
Measured	Fixed	Control variable
k_T	$n;\ p\ /\ \sigma_n$	$V_S\ /\ J_S$

3.2 Hull

The reference target case vessel, the Lürssen mega yacht in combination with the P3193 propeller, represents the main test case. The vessel features counter rotating propellers with a rotation direction of inwards over the top. In the model scale experimental campaigns, the length of the reference target case vessel is reduced at the middle frames to fit geometrically into the cavitation tunnel, which is expected to have negligible influence on the wakefield and thus both performance and acoustics. In both experiments and numerical investigations, the appendages, which are shaft brackets, a twisted rudder, as well as a diverging propeller hub cap are included in the model as shown in Figure 4 (a).

In the SINTEF cavitation tunnel and the numerical investigations in model scale (Table 3), a half-model is used, while the CNR-INM cavitation tunnel and the full scale experimental investigations consider a full-model, which leads to an additional difficulty in comparing the results between facilities, as a correction for the second propeller is required. Due to the highly different approaches followed within ProNoVi, an overview of the different methods used for the model scale investigations at C2 is provided in Table 4. All numerical calculations in model scale aim to copy the experimental measurements from the SINTEF cavitation tunnel. For full scale numerical investigations, a free-surface and a quasi-infinite domain parallel to the water surface and a water depth of around $40m$ are considered. Some additional analyses are undertaken with the other target case hulls and respective propellers described within the respective section.

Table 4 – Overview of methods for C2

Participant	Method	Geometry	Acoustics
Lürssen	Full scale exp.	Real vessel	Simulation of transmission losses
SINTEF	Model scale exp.	Cavitation tunnel, Half-model	Transfer function
CNR-INM	Model scale exp.	Cavitation tunnel, Full-model	Transfer function
SINTEF	FVM - StarCCM+	Quasi-infinite, Half-model (sym.)	Permeable surface FWH
Schottel	FVM - HELYX	Cavitation tunnel, Half-model	Permeable surface FWH
TUHH	Panel method -	Infinite, Wakefield	Permeable surface FWH

Besides the far-field observers, which are hydrophones located in the cavitation tunnels or held from a pilot boat respectively, there are nine pressure sensors on the hull above the propeller as indicated in Figure 4 (b) for all setups, except the full scale experiment. For the OpenFOAM setup, additionally the complete shown rectangular surface in (c) on the hull domain boundary is evaluated visually to provide a more intuitive way to assess propeller performance with respect to introduced hull pressure pulses.

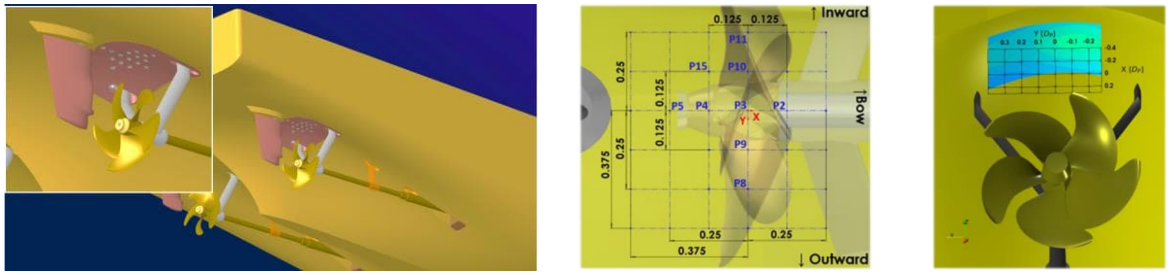

(a) Experimental model (b) pressure pick-ups (c) Evaluation boundary surface

Figure 4 – Hull observers locations

4. RESULTS

4.1 Cavitation Pattern

The cavitation pattern on the suction side for C2 (behind hull) reported in the model tests and in

the OpenFOAM and StarCCM+ setups are illustrated in Figure 5. A common occurrence is the leading-edge sheet cavitation starting at mid to outer radii sections and the increased cavitation volume at the 6 o'clock position. However, there is a disparity in reach of the sheet cavity with respect to the lower radii between the model test setups with one and two propellers. Another mentionable difference between both numerical approaches is the extent of cavity volume at the upwards rotating outer blade, which might be an effect of the different wakefield prediction between the setups. Other differences are the occurrence of a small hub vortex for the StarCCM+ setup, which interacts with the rudder bulb of the twisted rudder and a thin tip vortex filament for the SINTEF experiment for a geometrical length of half a rotation downstream of the propeller plane. The differences might have a large effect on predicted sound, even though the general occurrence of cavitation is identical between the methods.

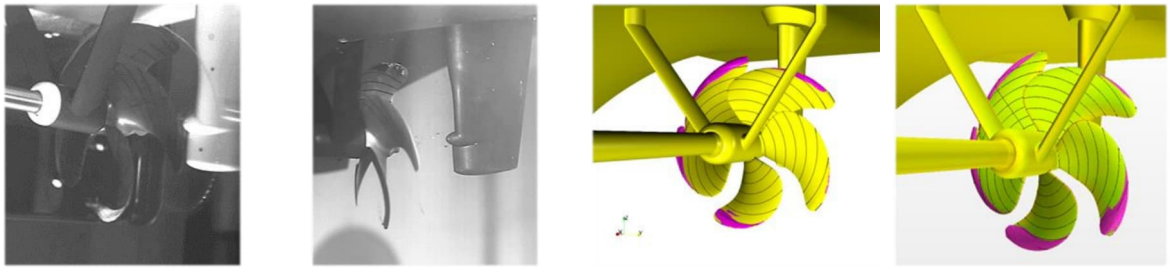

(a) Exp. SINTEF (b) Exp. CNR-INM (c) OpenFOAM LES (d) StarCCM+ DES

Figure 5 – Cavitation pattern with different methods, C2

4.2 Propeller Openwater Noise

For the different methods at the hydrophone location, a spectral representation of the radiated noise level scaled to $1m$ for the openwater case with the P1595 scaled to full scale is shown in Figure 6. In (a) the 1/3 octave bands from OpenFOAM, StarCCM+ and *pan*MARE are compared to the experimental results, which yields some agreement between $25 - 300Hz$. Only the OpenFOAM setup predicts SPL higher frequencies in a similar range than the model tests, while panMARE is technically not able to predict very high frequencies, StarCCM+ is generally underpredicting the noise, which might be a result of the quasi-infinite domain applied in this approach instead of a cavitation tunnel. In (b) the acoustic evaluation methods of direct pressure calculation within the domain and the FWH acoustic analogy are compared for OpenFOAM and *pan*MARE, which generally appear to yield similar results, which is expected and is considered a validation of this acoustic method. However, some unfavorable differences appear at the lower frequencies, especially the first two harmonics, which confirm that further research is required, since especially placement effects of the FWH control surface are not investigated in detail for this case. It is worth mentioning, that while the underlying data for both (a) and (b) is identical for the OpenFOAM case, the exact dominant frequency information causing the increased SPL, which might be important for the vessel operation, is lost in the 1/3 octave representation.

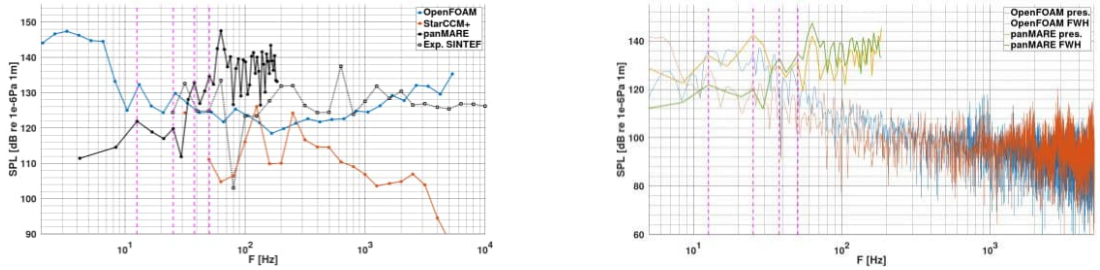

(a) 1/3 octave band results for methods with FWH (b) CFD domain pressure probes vs. permeable surface FWH observer

Figure 6 – Openwater P1595, Hydrophone location

4.3 Behind Hull Noise

For the analysis of the acoustic emissions with hull, initially the incompressible hull pressure at the pressure pick-ups on the hull at the first four propeller blade passing frequencies are summarized in Figure 7 for three locations P3, P4 and P10. At C2, wetted and cavitating condition are compared between the model scale setups for numerical and experimental methods with the amplitudes scaled

to full scale. Although the observer P3 is located directly above the propeller, other observers feature higher amplitudes, depending on the method. Another peculiarity is the reduced values in cavitating condition, which might be explained by the steady vapor volumes attenuating the acoustic emission and the low amount of trailing vortex cavitation at this operation point. In general, it is not possible to determine a clear trend, spatially between observer locations, methodically between approaches, or even between physics (wetted and cavitating). However, all approaches have in common that the higher blade harmonics are lower than the first, yet mostly underpredicted by numerical methods, except for OpenFOAM in cavitating condition, which might be a result of the LES turbulence modelling, although it has to be noted that the first harmonic is greatly overpredicted.

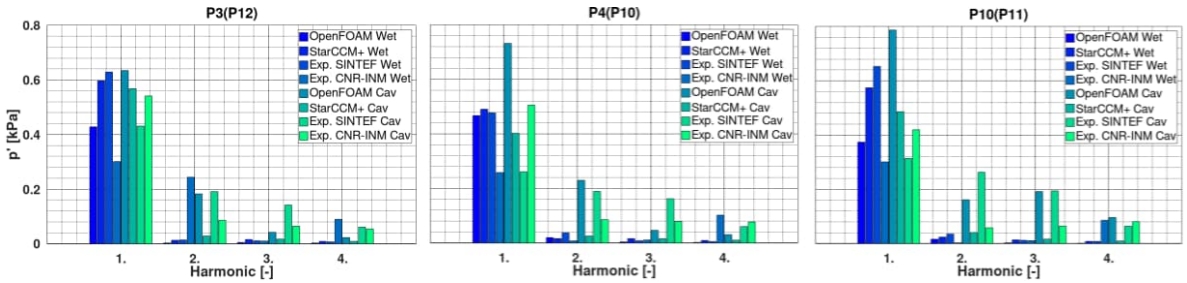

Figure 7 – Pressure fluctuations at propeller blade harmonics at selected hull observers, C2

In Figure 8, for the far-field, at the hydrophone location, the spectral radiated noise level is given in narrowband and 1/3 octave band representation for the model scale SINTEF cavitation tunnel obtained from OpenFOAM, StarCCM+ and the experiment. A good agreement between the octave bands is achieved between all methods over a wide frequency range from $60 - 2 \cdot 10^3 Hz$, even though the difference in narrowband is large due to the highly dissimilar sampling rates. In the low frequencies a clear resolution of the blade harmonics is only accomplished by OpenFOAM. At higher frequencies, an increase of acoustic pressure appears for StarCCM+, which might be explained by numerical issues. Similar to the openwater case, a clear allocation of the single sound contributions is only possible in narrowband representation.

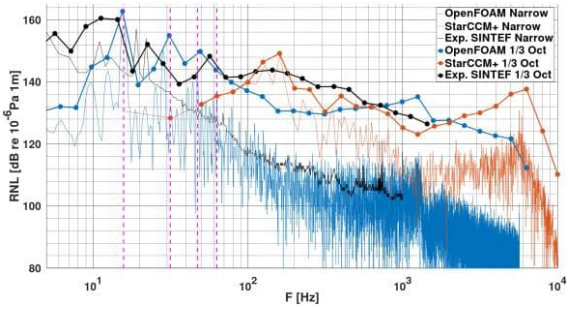

Figure 8 – Behind hull narrowband vs. 1/3 octave band, Hydrophone location, C2

4.4 Scaling Methods

For C1, the scaled results from the model scale experiments are compared to the full scale measurement in 1/3 octave bands in Figure 9 (a), where a correction is added to the SINTEF results in order to consider the full-model and the second working propeller. As a reference, the DNV Environment Transit limit curve (13) is given for which the vessel's measured signal is below for all approaches. Data points with background noise of not less than $3dB$ compared to the measured noise are omitted in the model test data. Due to cable vibrations the full scale results are disregarded below $100Hz$. In line with previous observations, single contributors are not discernible in this representation, while (b) shows the narrowband results for two full scale numerical approaches, where single contributions such as the harmonics or, in the case of the measurement, machinery are distinctly apparent. As a result of the lower level of detail of the panel method and the high timestep, the *pan*MARE results feature no high frequency or background noise. Here the vessel geometry is only considered as a wakefield, which might be an advantage to single out the propeller contributions due to the fundamental separation of propeller and vessel influence, such as in an optimization workflow.

The source of the high frequency noise around $1600Hz$ for the OpenFOAM approach is not clear and might be a numerical issue.

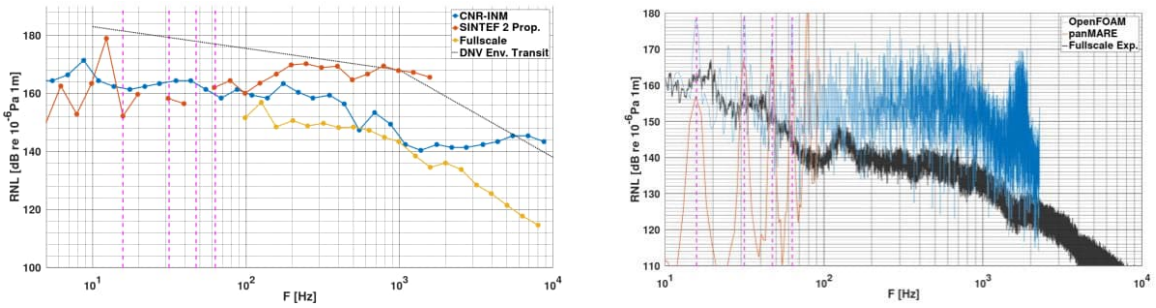

(a) EFD, model test facilities scaled to full scale, 1/3 octave band representation

(b) CFD with full scale setup and sea trial measurements

Figure 9 –Scaling methods, C1

4.5 Advanced Evaluation Methods

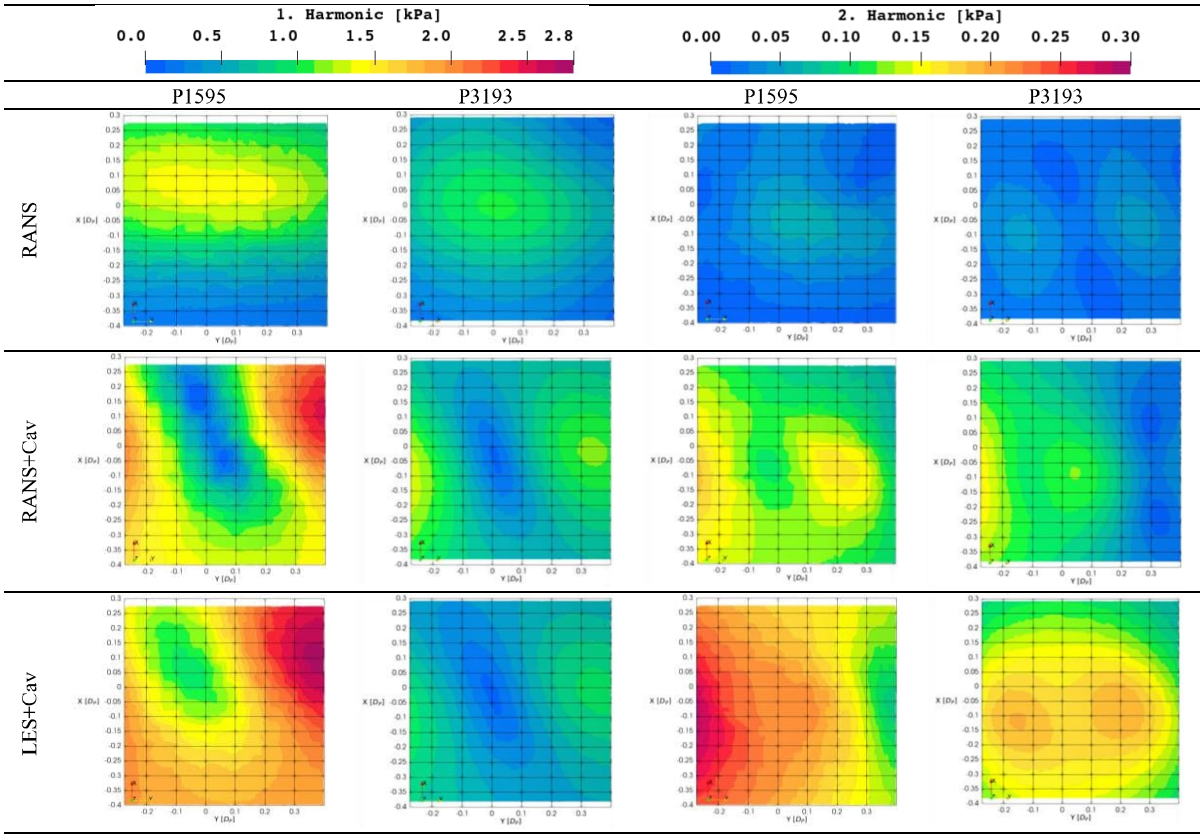

Figure 10 –Evaluation on simulation boundary patch, C1

For the OpenFOAM model scale simulations at C2, the boundary patch pressure pulse results for the first two propeller blade harmonics are visualized in Figure 10. The case is calculated with both propellers and thus have different frequencies for the harmonics. Compared to the representation as a bar graph in Figure 7, there is now a clear spatial pattern discernible and a trend between methods and in this case consideration of the level of physical details of the methods is identifiable. It is apparent and expected that there is a sound level change between wetted (RANS) and cavitating flow (RANS+Cav). While the first harmonic experiences no significant change between Reynolds-averaging (RANS+Cav) and resolving turbulent length scales (LES), the second harmonic is severely affected, which illustrates the necessity for adequate turbulence resolution at higher frequencies. It is expected that turbulence and turbulence-cavitation interaction, especially in the propeller slipstream is the source of noise at higher frequencies. In addition and for industrial applications most importantly, the characteristics of the propellers with respect to the sound input into the vessel hull are easily and clearly distinguishable.

4.6 Comparison of Vessel Signatures

All ProNoVi target case signatures at their respective design operation points are compared in Figure 11 in full scale, with the signals from individually placed observers normalized to $1m$ for comparability. The operation points are the above described C1 for the mega yacht ($v_S = 21kn,\ n = 188rpm$) with a power consumption of around $P \approx 11.000kW$, a vessel speed of $v_S = 18.5kn$ for the container vessel with a propeller diameter of $D_P = 5.8m$ and speed of $n = 111rpm$ and a power consumption of around $P \approx 7.800kW$, and for the wind farm service catamaran a vessel speed of $v_S = 19.9kn$ with a propeller diameter of $D_P = 0.98m$ and speed of $n = 780rpm$ and a power consumption of $P \approx 520kW$. The first two are evaluated with the described OpenFOAM setup, the latter with the StarCCM+ approach. Although there is a significant difference between vessel speeds and delivered power for the mega yacht and the container vessel the radiated noise levels are similar over a wide range of frequencies, which may be attributed to the twin-screw setup and noise optimized propellers for the yacht. The small catamaran on the other hand produces significantly less far-field noise with its small propellers, despite the high rate of rotation and subsequently similar propeller blade tip speed. Other possible explanations are due to underlying methods such as use of RANS, interference with "numerical noise" from the data interpolation on the sliding interface, and omission of all noise sources between the downstream boundary of propeller region and rudder for the FWH, which is an important area in the present case due to interaction between propeller slipstream and rudder, and rudder cavitation.

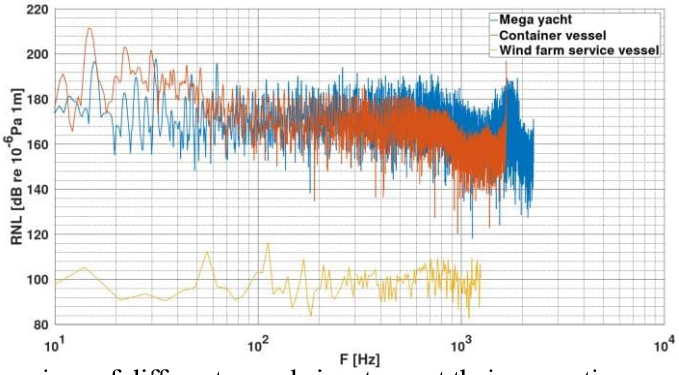

Figure 11 – Comparison of different vessel signatures at their respective operation points

5. DISCUSSION

5.1 Preferred Method

While model tests are considered state of the art for URN, the distinct differences between the facilities demonstrate some uncertainties. Full scale measurements on the other hand might not be representative and repeatable, as there is limited control over external test conditions. For highly iterative propeller design studies, the panel method *pan*MARE delivers adequate underwater noise results, especially when noise effect trends for the geometrical variation of propeller design parameters are desired. However, to resolve the propeller slipstream interactions and thus noise sources, high-fidelity CFD methods, such as FVM with resolution of the larger turbulent length scales is necessary. The studies prove that LES is preferable, however, the requirements regarding the simulation time-step and subsequently computational effort may be a feasibility constraint for widespread industry application at the moment. In addition, a noise signature evaluation requires several propeller rotations to resolve low frequency events sufficiently and to provide a good dataset for FFT analysis. Due to improved interpretability, a harmonic evaluation with high spatially resolved hull patches should be accepted as the new standard, in particular for numerical methods, as a result of easy implementation. It is clear from the comparison of vessel signatures, that the high-fidelity numerical methods are capable of obtaining meaningful comparative data between vessel types, which may be a feasible way to support broader studies by entities pursuing other research directions, such as analysis of regional or seasonal cumulative noise.

5.2 Open Issues and Directions of Future Research

Depending on the method there are different issues to resolve. For model tests, improved standards considering the test setup are required to increase accuracy and repeatability. The panel methods

shortcomings at the moment are primarily the lack of volume sources in the propeller slipstream due to the missing cavitating tip vortex and the interaction with the rudder. For the FVM approach, there are still several simplifications associated with the Schnerr-Sauer cavitation model, however, it is expected that ultimately the VOF two-phase treatment might not be sufficient for high frequency noise, as single bubble implosions are the primary contributors depending on the bubble radius, requiring Euler-Lagrange coupling. Other shortcomings are the resolution of the cavitating tip vortex, which is the current bottleneck in setting up simulations and computational effort, meaning that advanced meshing strategies such as smart and automatic adaptive mesh refinement are the next step in this technological evolution.

6. SUMMARY

Different propeller geometries have been investigated regarding underwater radiated noise in openwater and behind hull condition in model and full scale. The approaches consist of two different size model scale test facilities with a half- and a full-model, a full scale measurement, a panel method and two software distributions for FVM. Generally, the results of all methods are in a good agreement range with respect to each other, confirming all as feasible ways forward, however, shortcomings regarding the accuracy are found. Notably the comparison of equal setups in experiment and numerical investigations, such as the model scale C2 and full scale C1 comparison, illustrate the remaining difficulties.

ACKNOWLEDGEMENTS

The authors are very grateful for the support and funding by MarTERA, represented by BMWi-project (03SX461C) "ProNoVi" for the German partners, the Research Council of Norway for the Norwegian Partners (Project 284501) and MIUR-project "ProNoVi" for the CNR-INM.

REFERENCES

1. Frisk GV. Noiseonomics: The relationship between ambient noise levels in the sea and global economic trends. Scientific Reports; 2012.
2. Branstetter BK, Leger JS, Acton D, Stewart J, Houser D, Finneran JJ, et al. Killer whale (Orcinus orca) behavioral audiograms. The Journal of the Acoustical Society of America. 2017;4.
3. O'Hara J, Wilcox J. Avoidance Responses of Loggerhead Turtles, Caretta caretta, to Low Frequency Sound. Copeia. 1990;6:564–7.
4. Casper BM, Lobel PS, Yan HY. The hearing sensitivity of the little skate, Raja erinacea: A comparison of two methods. Environmental Biology of Fishes. 2003;8.
5. IMO. Guidelines for the Reduction of Underwater Noise from Commercial Shipping to Address Adverse Impacts on Marine Life. 2014.
6. Port of Vancouver Vancouver Fraser Port Authority, editor. ECHO Program 2021 Annual report. 2022.
7. Kimmerl J, Mertes P, Abdel-Maksoud M. Application of Large Eddy Simulation to Predict Underwater Noise of Marine Propulsors. Part 1 Cavitation Dynamics. Journal of Marine Science and Engineering. 2021;(778).
8. Krasilnikov V. CFD modelling of hydroacoustic performance of marine propellers: Predicting propeller cavitation. Proceedings of the 22nd Numerical Towing Tank Symposium. 2019;
9. Schnerr GH, Sauer J. Physical and Numerical Modeling of Unsteady Cavitation Dynamics. 4th International Conference on Multiphase Flow. 2001;
10. Katz, Plotkin A, Plotkin J. Low-Speed Aerodynamics. 2nd ed. Cambridge, USA: Cambridge University Press; 2001.
11. Fine NE. Nonlinear Analysis of Cavitating Propellers in Nonuniform Inflow. Cambridge, USA: Massachussetts Institute of Technology; 1992.
12. Francescantonio P. A New Boundary Integral Formulation For The Prediction Of Sound Radiation. Journal of Sound and Vibration. 1997;
13. DNV GL AS, editor. DNV-GL Rules for Classification Ships, Part 6 Additional class notations Chapter, 7 Environmental protection and pollution control. 2017.